

Alma Mater Studiorum Università di Bologna  
Archivio istituzionale della ricerca

Piezoelectric properties of PVDF-TrFE/BaTiO<sub>3</sub> composite foams with different contents of TrFE units

This is the final peer-reviewed author's accepted manuscript (postprint) of the following publication:

*Published Version:*

Kubin M., Makreski P., Zanoni M., Selleri G., Gasperini L., Fabiani D., et al. (2023). Piezoelectric properties of PVDF-TrFE/BaTiO<sub>3</sub> composite foams with different contents of TrFE units. POLYMER COMPOSITES, 44(11), 7804-7816 [10.1002/pc.27667].

*Availability:*

This version is available at: <https://hdl.handle.net/11585/957396> since: 2024-02-13

*Published:*

DOI: <http://doi.org/10.1002/pc.27667>

*Terms of use:*

Some rights reserved. The terms and conditions for the reuse of this version of the manuscript are specified in the publishing policy. For all terms of use and more information see the publisher's website.

This item was downloaded from IRIS Università di Bologna (<https://cris.unibo.it/>).  
When citing, please refer to the published version.

(Article begins on next page)

# Piezoelectric properties of PVDF-TrFE/BaTiO<sub>3</sub> composite foams with different contents of TrFE units

*Mateja Kubin<sup>1</sup>, Petre Makreski<sup>2</sup>, Michele Zannoni<sup>3</sup>, Giacomo Selleri<sup>4</sup>, Leonardo Gasperini<sup>4</sup>, Davide Fabiani<sup>4,5</sup>, Chiara Gualandi<sup>3,5</sup>, Aleksandra Bužarovska<sup>1\*</sup>*

<sup>1</sup>Ss Cyril and Methodius University, Faculty of Technology and Metallurgy, Rudjer Boskovic 16, 1000 Skopje, N. Macedonia

<sup>2</sup>Ss. Cyril and Methodius University, Faculty of Natural Sciences and Mathematics, Institute of Chemistry, Arhimedova 5, 1000 Skopje, N. Macedonia


<sup>3</sup>Department of Chemistry “Giacomo Ciamician” and INSTM UdR of Bologna, University of Bologna, Via Selmi, 2, 40126 Bologna, Italy

<sup>4</sup>Department of Electrical, Electronic, and Information Engineering, University of Bologna, Viale Risorgimento 2, 40136 Bologna, Italy

<sup>5</sup>Interdepartmental Center for Industrial Research on Advanced Applications in Mechanical Engineering and Materials Technology, CIRI-MAM, University of Bologna, Viale Risorgimento, 2, 40136 Bologna, Italy

## Correspondence

Aleksandra Bužarovska - Ss Cyril and Methodius University, Faculty of Technology and Metallurgy, Rudjer Boskovic 16, 1000 Skopje, N. Macedonia;

 0000-0002-6512-4165; E-mail: [abuzar@tmf.ukim.edu.mk](mailto:abuzar@tmf.ukim.edu.mk)

## Abstract

Piezoelectric materials play an important role in the emerging field of micro and wearable electronics. Achieving high piezoelectric response is a key feature for their use in energy harvesting and sensing systems. In this study, highly porous lightweight composite foams composed of PVDF-TrFE (70/30 and 80/20 mol%) and different BaTiO<sub>3</sub> content (5, 10 and 20 wt.%) are prepared by thermally induced phase separation method (TIPS). The piezoelectric foams were structurally and thermally examined by using FTIR, XRD, DSC, and TGA analyses. All composite foams were characterized by high  $\beta$ -phase content, while the addition of ceramic particles resulted in higher crystallinity and thermal stability of the investigated foams. Two distinct poling methods were employed due to the different molar compositions of the copolymers. The piezoelectric response was measured by the piezoelectric strain coefficient ( $d_{33}$ ) and the output current ( $I_p$ ). The composite foams based on PVDF-TrFE 70/30 mol% copolymer, having two well-separated Curie temperatures for the organic and inorganic phases, can be polarized to achieve the contribution of both components to the piezoelectric performance, reaching the highest value of  $-28.3 \text{ pC N}^{-1}$  and 130 nA at 10 Hz for the composite with 20 wt.% BaTiO<sub>3</sub>.

**KEYWORDS** PVDF-TrFE, BaTiO<sub>3</sub>, poling, piezoelectric composite foams

## 1 INTRODUCTION

In the last 15 years, a significant scientific focus was given to piezoelectric (PE) materials capable to convert mechanical stresses into electricity under certain conditions.<sup>1</sup> Although various PE materials from different origins were already developed, there is a huge interest in creating new piezo systems with improved properties. Poly(vinylidene fluoride) (PVDF) and its derived copolymers as typical representatives of the polymer piezoelectrics were widely explored due to their flexibility, biocompatibility, and easy processing.<sup>2-5</sup> However, they possess lower piezoelectric constants when compared to piezoceramics which also limits their wider use.

PVDF as an important piezo polymer can crystallize in five different polymorphs ( $\alpha$ ,  $\beta$ ,  $\gamma$ ,  $\delta$  and  $\epsilon$ ), among which  $\alpha$  and  $\epsilon$  are non-polar phases, while  $\beta$ ,  $\gamma$ , and  $\delta$  are polar ones.<sup>6</sup> The  $\beta$  phase of PVDF shows the highest piezoelectric response among all phases and its development is favoured under particular processing conditions.<sup>7</sup> Random copolymers of PVDF, poly(vinylidene

fluoride-*co*-trifluoroethylene) (PVDF-TrFE), possess higher piezoelectric constants, due to their ability to readily crystallize in the  $\beta$  crystal phase. Namely, the introduction of additional fluorine atoms arising from the TrFE units hinders the formation of *tgtg'* conformation typical for the  $\alpha$  phase and allows the copolymer to crystallize in the all-trans conformation relevant for the  $\beta$  crystal structure.<sup>8</sup>

Based on these facts, PVDF-TrFE copolymers have been widely used for the production of films, nanofibers, and nanowires via various processes, such as spin-coating, solution casting, electrospinning, nanoimprinting, etc.<sup>9-12</sup> Although PVDF-TrFE copolymers crystallize mainly in  $\beta$  phase, achieving a high piezoelectric response is still a challenging task since the development of a highly desired  $\beta$  phase is necessary but not a sufficient condition.

Therefore, various strategies have been used to improve the degree of crystallinity and piezoelectric response of PVDF-TrFE copolymers.<sup>13</sup> One approach to improve piezoelectricity is to incorporate piezoelectric ceramic particles into the polymer matrix. Barium titanate ( $\text{BaTiO}_3$ ), as a lead-free piezo ceramic with high dielectric and piezoelectric constants, is frequently used as a filler in piezoelectric polymers.<sup>14-17</sup> PVDF-TrFE composites with embedded  $\text{BaTiO}_3$  particles demonstrated improved piezoelectric charge, current outputs, and power densities ascribable both to the nucleating effect of  $\text{BaTiO}_3$ , increasing  $\beta$  phase crystallization kinetics and to the improved interfacial polarization.<sup>18,19</sup> A high-performance flexible piezoelectric nanogenerator composed of a micro-pillar PVDF-TrFE/ $\text{BaTiO}_3$  array was produced by the nanoimprinting process showing significantly enhanced voltage and current-voltage density compared to the pristine polymer.<sup>18</sup> Furthermore, PVDF-TrFE/ $\text{BaTiO}_3$  nanofibers coupled with penetrated electrodes showed enhanced sensing performance.<sup>19</sup>

Another approach for enhancing the piezoelectric response of piezopolymers is by altering their structure. The porous structure within the polymer was found to promote electromechanical coupling efficiency, leading to an increase in compressibility, and improved sensitivity of the mechanical inputs. Accordingly, porous films of PVDF-TrFE, produced as an upper layer in a multilayered polymer film structure using the phase separation method, were shown to have 107% higher maximum voltage than solid films. The increased local stress within the porous structure was found to have a significant effect on the increased output voltage.<sup>20</sup> A similar method of fabrication of PVDF-TrFE 3D porous structure films was published by Chen et al.<sup>21</sup> It was shown that the increased pore size has the effect to increase the output voltage,

demonstrating films with better piezoelectric performances. Apart from the phase separation method, template methods can be used to achieve a high porosity structure. Open-cell electro-conductive PVDF-TrFE/MWCNTs nanocomposite foams obtained using the sugar-templating method were characterized by an enhanced sound absorption coefficient in noise mitigation applications.<sup>22</sup> An additional key advantage provided by porous materials is their lower density compared to their bulk counterparts, which encourages their application as lightweight wearable devices.

In this study, we have prepared PVDF-TrFE/BaTiO<sub>3</sub> composite foams doped with different ceramic filler contents, using the thermally induced phase separation method (TIPS). The main objective of this work was to investigate the effect of foam porosity, ceramic particle content and molar composition of the used copolymers on the morphological, thermal, structural, and piezoelectric behavior of PVDF-TrFE/BaTiO<sub>3</sub>. Special attention was given to poling treatments considering the different Curie temperatures of the applied materials.

## **2 MATERIALS AND METHODS**

### **2.1 Materials**

PVDF-TrFE copolymer (Solvene 300/P300) with 30 mol% TrFE and PVDF-TrFE copolymer (Solvene 200/P400) with 20 mol% TrFE were purchased from Sigma Aldrich. BaTiO<sub>3</sub> (IV) (99%) powder with an average particle size of 0.85 - 1 μm was supplied from Acros Organics. Dimethyl sulfoxide (DMSO) with a purity of 99.5 % (Merck product) was used as a solvent for the preparation of composite foams. Distilled water and ethanol (96 %) (Alkaloid product) were used as non-solvent baths.

### **2.2 Sample preparation**

PVDF-TrFE/BaTiO<sub>3</sub> composite foams were prepared using the TIPS method, applying a freeze extraction process to remove the frozen solvent. The polymer solutions were prepared by individually dissolving PVDF-TrFE powders in DMSO at a concentration of 5% w/v, by magnetic stirring at 50 °C for 6 h. DMSO was chosen as a suitable solvent due to its high freezing point of 19 °C. BaTiO<sub>3</sub> powder of 5, 10, and 20 wt.% in respect to the composite, was

added to the polymer solutions, and ultrasonically treated for 1 h in an ultrasonic bath. The dispersions were poured into Petri dishes ( $d = 4$  cm) with Teflon® tape-protected side walls and placed on a cold metal plate in a freezer at a temperature of  $-30$  °C. After 24 h the frozen samples were submerged in a water bath for two consecutive days and subsequently in an ethanol bath to completely extract the solvent and create a porous morphology. The resulting composite foams were air-dried at room temperature (RT) and labelled as presented in Table 1.

**Table 1.** Sample abbreviations and composition of PVDF-TrFE/BaTiO<sub>3</sub> composite foams

Sample code	PVDF:TrFE mol%	PVDF-TrFE/BaTiO <sub>3</sub> wt%
PVDF-TrFE(30)	70:30	100/0
PVDF-TrFE(30)-5	70:30	95/5
PVDF-TrFE(30)-10	70:30	90/10
PVDF-TrFE(30)-20	70:30	80/20
PVDF-TrFE(20)	80:20	100/0
PVDF-TrFE(20)-5	80:20	95/5
PVDF-TrFE(20)-10	80:20	90/10
PVDF-TrFE(20)-20	80:20	80/20

### 2.3 Poling of composites

The poling process was performed by applying a high electric field to all the specimens, which were placed between an electrode connected to a high-voltage generator and a ground plate. The whole process was carried out in an ester oil bath (FR3 natural ester, Cargill, electrical breakdown =  $70$  kV mm<sup>-1</sup>), as described in detail in Figure 1a. Before polarization, samples were immersed in oil and placed in a vacuum chamber to eliminate air bubbles. Due to the discrepancy of piezoelectric coefficients of BaTiO<sub>3</sub> and P(VDF-TrFE), and taking into account the different Curie temperatures ( $T_c$ ) of the constituents, two different poling methods were adopted. PVDF-TrFE(20) composite foams were poled at  $120$  °C for 60 min by applying  $+20$  kV mm<sup>-1</sup> to the samples, while a two-step poling process was applied to the PVDF-TrFE(30) composite foams. In the latter case, first, a negative electric field of  $-15$  kV mm<sup>-1</sup> was applied for 30 min at  $120$  °C, then the temperature was gradually decreased to  $100$  °C and the electric field polarity was switched to  $+20$  kV mm<sup>-1</sup> for 30 min. At the end of poling treatments, the

temperature was decreased to RT while keeping the electric field on. To fully remove the oil, all the specimens were soaked in a cyclohexane bath for 1 h.

## 2.4 Characterization of PVDF-TrFE/BaTiO<sub>3</sub> composite foams

The morphology and the pore structure of the prepared foams and the distribution of BaTiO<sub>3</sub> particles were evaluated using a Scanning Electron Microscope (SEM, Leica Cambridge Stereoscan 360) operating at an accelerating voltage of 20 kV. Before observations, the samples were coated with gold.

The density and porosity of the prepared foams were measured by the liquid displacement method using ethanol as a medium.<sup>23</sup> The density ( $\rho$ ) and the porosity ( $\varepsilon$ ) were determined using the following equations:

$$\rho = \frac{W}{V_2 - V_1} \quad (1)$$

$$\varepsilon = \frac{V_1 - V_3}{V_2 - V_3} \times 100 \quad (2)$$

where  $W$  is the weight of the polymer foam,  $V_1$  is the initial volume of ethanol contained in the glass vial,  $V_2$  is the total volume of ethanol and ethanol-impregnated foam and  $V_3$  is the volume of the residual ethanol in the vial, after removing the ethanol-impregnated polymer foams.

The crystalline phases in PVDF-TrFE/BaTiO<sub>3</sub> composite foams were analyzed using attenuated total reflectance Fourier Transform Infrared Spectroscopy (ATR-FTIR) (IRAffinity-1S, Shimadzu spectrometer, Japan). The measurements were performed in the wavenumber range of 4000 cm<sup>-1</sup> - 400 cm<sup>-1</sup>, with a scan number of 32 and a resolution of 4 cm<sup>-1</sup>.

XRD measurements were performed using a Rigaku Ultima IV powder X-ray diffractometer, at RT in the  $2\theta$  range of 10 - 80°, with a scan rate of 0.02 min<sup>-1</sup>. CuK $\alpha$  ( $\lambda$  = 0.154 nm) radiation was obtained from a generator set at 40 kV and a current of 40 mA.

Thermogravimetric analysis was performed using TGA Q500 (TA instruments) under constant air flow. The measurements were performed from RT to 600 °C with a heating rate of 10 °C min<sup>-1</sup>.

TA Instruments differential scanning calorimeter, DSC Q2000, equipped with a refrigerated cooling system (RCS) was used for DSC analysis. A first heating scan was performed in a temperature range of -90 - 200 °C with a heating rate of 10 °C min<sup>-1</sup>; samples were then cooled to

-90 °C with a cooling rate of 10 °C min<sup>-1</sup>, and reheated up to 200 °C with the same heating rate of 10 °C min<sup>-1</sup>.

## 2.5 Piezoelectric measurements

The piezoelectric performances of the composite foams were evaluated by measuring the piezoelectric strain coefficient  $d_{33}$  (pC N<sup>-1</sup>) and the output current. The  $d_{33}$  was measured with the piezometer ( $d_{33}$  PiezoMeter System PM300, Piezotest, Singapore). The output current was acquired by an electrometer (Keithley 6517B, input impedance >200 T $\Omega$ ) in response to a compressing sinusoidal force oscillating between 0 N and 80 N at different frequencies (2, 5 and 10 Hz), as shown in Figure 1b. The cylindrical brass indenter (diameter equal to 1.4 cm) was used as an electrode to collect the output current and was connected to the input channel of the electrometer.

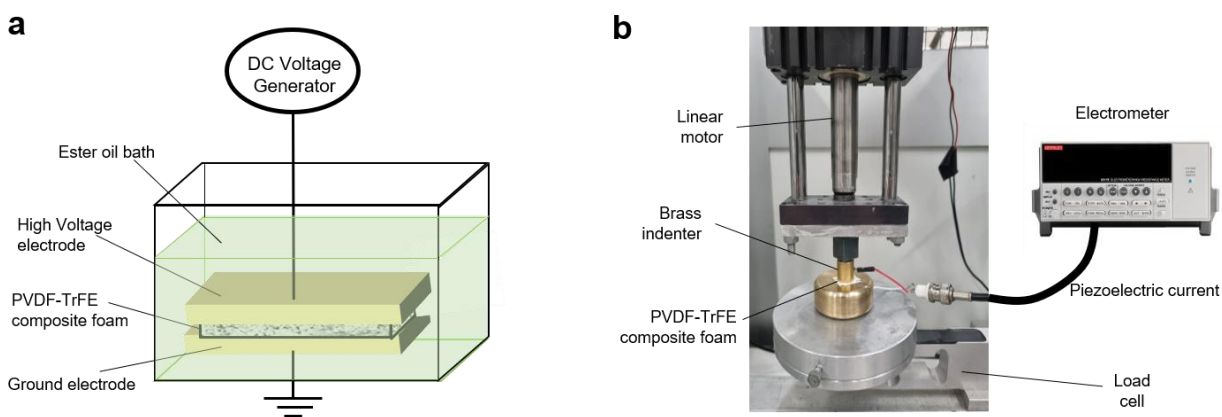


**Figure 1.** Poling setup (a) and setup for current measurements (b).

## 3 RESULTS AND DISCUSSION

### 3.1 Morphological analysis

The composite foams with thickness of around 500  $\mu\text{m}$  were produced by TIPS and some of their representative SEM images are reported in Figure 2. Foams are all characterized by a tortuous porosity with open irregular cells in the order of tens of microns. A close inspection at high magnification allows the visualization of particles with micrometric and sub-micrometric



diameters (Figure 2f). Typically, the TIPS fabrication method leads to the production of polymer foams with very well-distributed micro- and nanoparticles without agglomeration. This is mainly a result of the rapid freezing process of polymer dispersions, which does not allow the formation of larger agglomerates.<sup>24,25</sup>

Porosity and density data of all fabricated foams are collected in Table 2. The PVDF-TrFE(30) and its composite foams had a porosity of around 92% and almost constant densities of 0.15 g cm<sup>-3</sup>. Higher densities (0.18-0.20 g cm<sup>-3</sup>) and lower porosities in the range of 85.2-89.2% were determined for PVDF-TrFE(20) composite foams. This data is consistent with the previous published results, where the polymer concentration of 5 wt.% generally leads to high porosities between 86 and 93 %.<sup>24,25</sup>

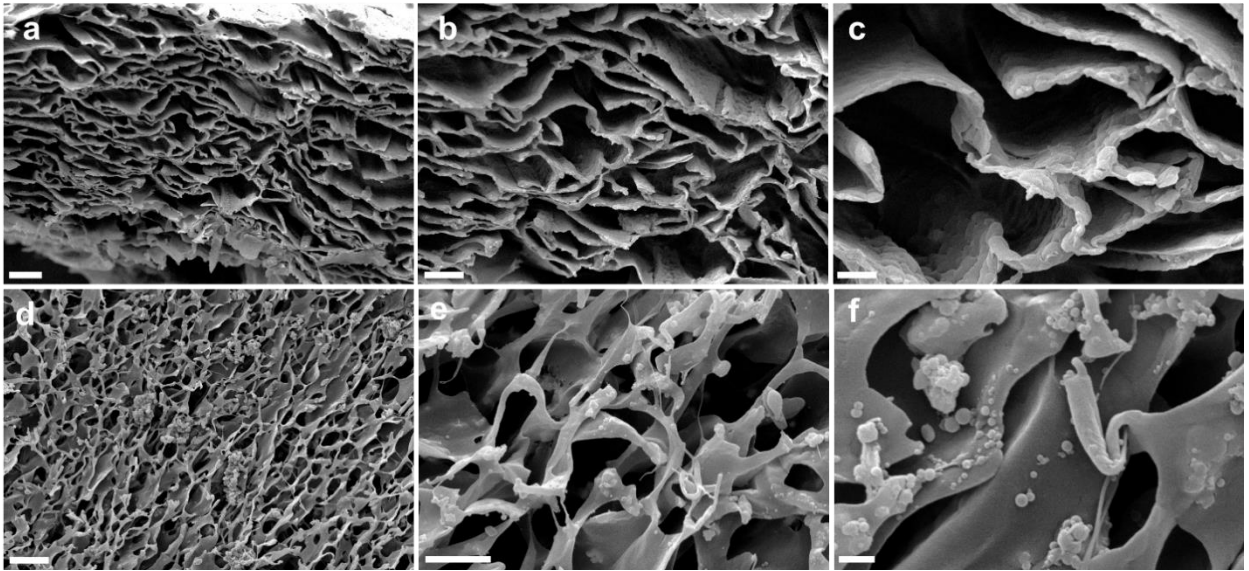


**Figure 2.** Representative SEM images of PVDF-TrFE/BaTiO<sub>3</sub> composite foams: cross-section (a-c) and surface view (d-f). Scale bars: 20 μm (a), 10 μm (b, d), 4 μm (c), 5 μm (e) and 1 μm (f).

**Table 2.** Density and porosity calculations of PVDF-TrFE/BaTiO<sub>3</sub> foams.

Sample code	$\rho^a$ [g cm <sup>-3</sup> ]	$\epsilon^b$ [%]
PVDF-TrFE(30)	0.15±0.02	91.7±0.01
PVDF-TrFE(30)-5	0.14±0.01	92.4±0.03

PVDF-TrFE(30)-10	0.15±0.01	89.9±0.03
PVDF-TrFE(30)-20	0.15±0.01	91.5±0.02
PVDF-TrFE(20)	0.18±0.03	85.2±0.03
PVDF-TrFE(20)-5	0.19±0.03	94.6±0.01
PVDF-TrFE(20)-10	0.19±0.01	86.2±0.01
PVDF-TrFE(20)-20	0.20±0.02	89.5±0.03

<sup>a</sup> Calculated by applying Eq. (1).

<sup>b</sup> Calculated by applying Eq. (2).

### 3.2 FTIR spectroscopy characterization

ATR-FTIR analysis was performed to evaluate the presence of different polymorphs and to determine the relative content of  $\beta$  crystal phase evolved during the crystallization process of PVDF-TrFE/BaTiO<sub>3</sub> composite foams. FTIR spectra of both PVDF-TrFE(30)/BaTiO<sub>3</sub> and PVDF-TrFE(20)/BaTiO<sub>3</sub> composite foams are presented in Figure 3. FTIR spectra of PVDF-TrFE(30) and its composites showed a strong band at 837 cm<sup>-1</sup> (CF<sub>2</sub> symmetric stretch) exclusively relevant for  $\beta$ -phase. Characteristic bands of the  $\beta$  phase crystals had been also identified at 1392 cm<sup>-1</sup>, 1276 cm<sup>-1</sup>, and 1076 cm<sup>-1</sup> (appeared as shoulder peak) corresponding to *all-trans* chain conformation, while the band at 1111 cm<sup>-1</sup> (indicated with a triangle) was closely correlated to vibrational modes localized on the TrFE units.<sup>26,27</sup> Additional peaks at 1165, 873 and 500 cm<sup>-1</sup> were also observed and, according to literature data, their presence is usually ascribed to the  $\beta$  phase or mixed  $\beta/\gamma$  phase.<sup>27,28</sup> The absorption peak identified at 1234 cm<sup>-1</sup> confirmed the presence of the  $\gamma$  crystal phase.<sup>29</sup> With a careful inspection of the FTIR spectra, no characteristic peaks relevant for  $\alpha$  phase could be identified, except the almost minor intensity peak positioned at 766 cm<sup>-1</sup>, originating from CF<sub>2</sub> and skeletal bending vibrations of the TGTG' conformation of the  $\alpha$  phase.<sup>26,30</sup> The addition of micro-sized BaTiO<sub>3</sub> in the corresponding copolymer matrix does not influence the bands shifting, since no specific interactions between the filler and the matrix were expected.

The FTIR spectra of the composite foams based on PVDF-TrFE(20) display the same characteristic peaks relevant for the  $\beta$  crystal phase as shown by PVDF-TrFE(30) foams, while their wavenumbers were shifted to slightly lower values. It is also interesting to point out that the shoulder band positioned at 1076 cm<sup>-1</sup> in the spectrum of PVDF-TrFE(30) (Figure 3a), appears in

PVDF-TrFE(20) copolymer as a sharp separate peak located at 1068 cm<sup>-1</sup> (Figure 3b). The relative content of the  $\beta$  phase,  $F(\beta)$  for both systems was determined using the equation:

$$F(\beta) = \frac{A_{\beta}}{\left(\frac{K_{\beta}}{K_{\alpha}}\right)A_{\alpha} + A_{\beta}} = \frac{A_{\beta}}{1.26A_{\alpha} + A_{\beta}} \times 100 \quad (3)$$

where the absorption coefficients,  $K_{\alpha}$  and  $K_{\beta}$  are  $6.1 \times 10^4$  and  $7.7 \times 10^4$  cm<sup>2</sup> mol<sup>-1</sup>, while  $A_{\alpha}$  and  $A_{\beta}$  are absorbances at 766 cm<sup>-1</sup> and 837 cm<sup>-1</sup>, respectively.<sup>31</sup> The results collected in Table 3 clearly showed that the copolymers and composite foams were characterized by very high contents of  $\beta$  phase, between 95.4 and 98.4%, when compared to literature data where  $F(\beta)$  ranges between 65 to 88 %.<sup>12,15,19</sup> The content of the  $\beta$  phase was approximately the same for both copolymers and the addition of BaTiO<sub>3</sub> was found to have a minor impact on the increased content of the  $\beta$  phase. These findings suggested that the high  $F(\beta)$  values relevant for all foams are mostly influenced by the content of TrFE units and processing parameters rather than by the content of BaTiO<sub>3</sub>. Furthermore, using a solvent with a high dipole moment, such as DMSO, was found to promote the regular orientation of the polymer's chains and the  $\beta$  phase formation.<sup>32</sup>

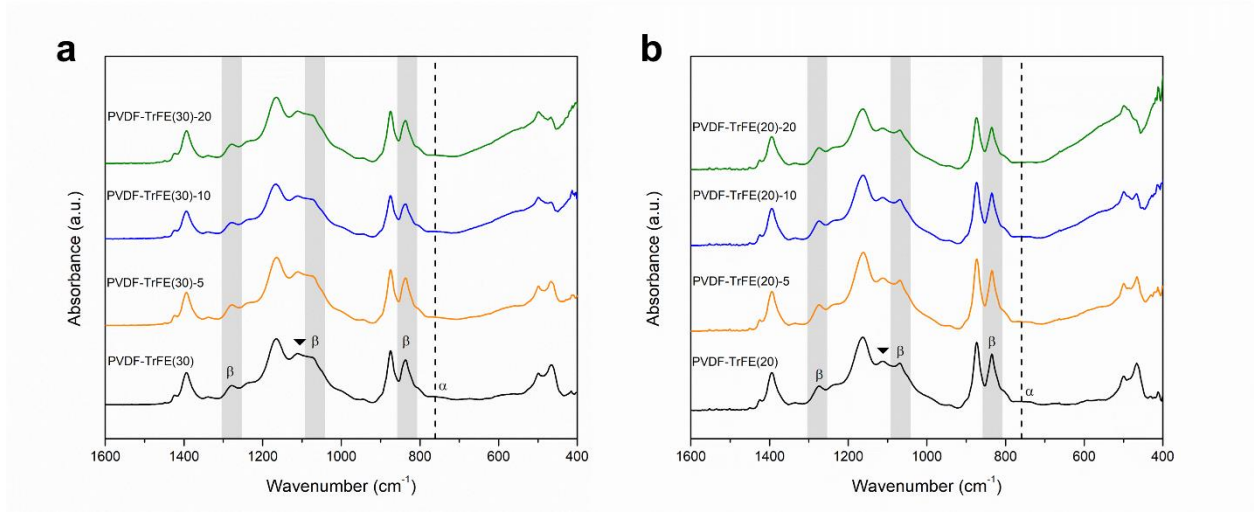


**Figure 3.** ATR-FTIR spectra of (a) PVDF-TrFE(30)-BaTiO<sub>3</sub> composite foams and (b) PVDF-TrFE(20)-BaTiO<sub>3</sub> foams.

### 3.3 Microstructural analysis

XRD diffraction was performed to study the crystalline structure of the as-prepared composite foams. XRD diffraction patterns of the pure PVDF-TrFE(30), and PVDF-TrFE(20) copolymers and their composites foams are shown in Figure 4. The pattern of PVDF-TrFE(30) copolymer

(Figure 4a) was characterized by an intense peak located at  $19.8^\circ$ , corresponding to the overlapped (110) and (200) planes of the  $\beta$  crystal phase.<sup>33,34</sup> The two additional peaks located at  $35^\circ$  and  $40.7^\circ$  are also attributed to the  $\beta$  phase of pure copolymer corresponding to (001) and (201, 111) planes, respectively.<sup>33</sup> In the XRD pattern of PVDF-TrFE(20) (Figure 4c) the intense peak attributed to the  $\beta$  phase was observed at  $20.1^\circ$ . Other reflections in the region of  $30-45^\circ$  can be also seen but with increased intensity, indicating a more ordered  $\beta$  phase in the copolymer with a higher content of VDF.<sup>33,34</sup> The diffraction peaks of the perovskite structure of  $\text{BaTiO}_3$  belonging to the (100), (110), (111), and (200) orientation planes were observed at  $22.2^\circ$ ,  $31.5^\circ$ ,  $38.9^\circ$ , and  $45.3^\circ$ , respectively, increasing their intensity with increasing the content of  $\text{BaTiO}_3$  in the corresponding composite foams.<sup>35</sup> The pronounced shoulder to the main peak, observed at  $19.8^\circ$  in PVDF-TrFE(30) and at  $20.1^\circ$  in PVDF-TrFE(20), was an indication of the presence of an amorphous phase in both copolymers.<sup>36</sup> Curve deconvolution was carried out by using a combination of Gaussian and Lorentzian distribution functions (Figure 4b and 4d). The degree of crystallinity was then calculated from the ratio between the integrated crystalline peaks and the total area of crystalline peaks and amorphous halo. The degree of crystallinity of the unfilled PVDF-TrFE(30) copolymer foam was 45.6% (Table 3), while the addition of  $\text{BaTiO}_3$  contributed to increased crystallinity, reaching the highest value of 65.1% for the composite foam filled with 10 wt.% of  $\text{BaTiO}_3$ . Higher degrees of crystallinity were characteristic for PVDF-TrFE(20) copolymer and its composite foams between 50.7 and 74.5%, clearly showing increased crystallinity with higher content of  $\text{BaTiO}_3$ . PVDF-TrFE(20) foams showed higher crystallinity when compared to PVDF-TrFE(30) foams, thus suggesting a more ordered  $\beta$  phase in the former.

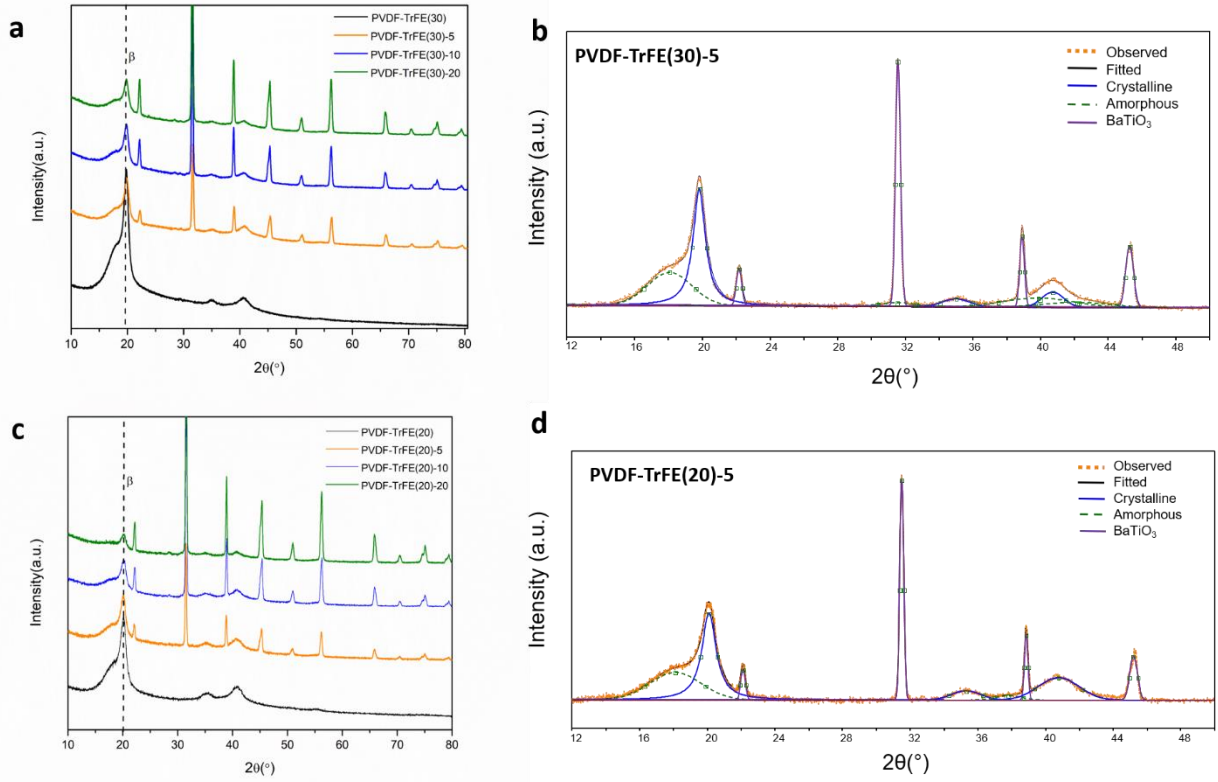


**Figure 4.** XRD pattern of PVDF-TrFE(30)-BaTiO<sub>3</sub> composite foams (a) and corresponding curve fitting (b); XRD pattern of PVDF-TrFE(20)-BaTiO<sub>3</sub> foams (c) and corresponding curve fitting (d).

**Table 3.** FTIR and XRD analyses of PVDF-TrFE/BaTiO<sub>3</sub> composite foams.

Sample code	F( $\beta$ ) <sup>a</sup> [%]	X <sub>c</sub> [%]
PVDF-TrFE(30)	95.4	45.6
PVDF-TrFE(30)-5	97.2	54.1
PVDF-TrFE(30)-10	96.2	65.1
PVDF-TrFE(30)-20	96.5	63.7
PVDF-TrFE(20)	96.6	50.7
PVDF-TrFE(20)-5	96.6	66.6
PVDF-TrFE(20)-10	96.8	70.0
PVDF-TrFE(20)-20	98.4	74.5

<sup>a</sup> Calculated by applying Eq. (3).

### 3.4 Thermal properties

TGA thermograms of all investigated samples are presented in Figure 5a and 5b and all relevant data obtained from the TGA curves are summarized in Table 4. A two-step degradation path in the temperature range of 400-550 °C was characteristic for both copolymer foams.<sup>37</sup> On the other hand, BaTiO<sub>3</sub>, like most inorganic materials, is stable within the whole temperature range with a very low weight loss of 0.7%. The residual weights of 0.6% and 0.2% at 600 °C were determined for PVDF-TrFE(30) and PVDF-TrFE(20) copolymer foams respectively, while gradually increased values, consistent with the nominal content of BaTiO<sub>3</sub>, were detected in the composite foams. It could be also noted that the onset decomposition temperatures were moved to higher values when compared to those recorded for PVDF-TrFE(30) (at 452°C) and PVDF-TrFE(20) (455 °C) copolymers. This result suggests that the addition of BaTiO<sub>3</sub> increased the thermal stability of the polymer in the composite foams, as previously found.<sup>38</sup>

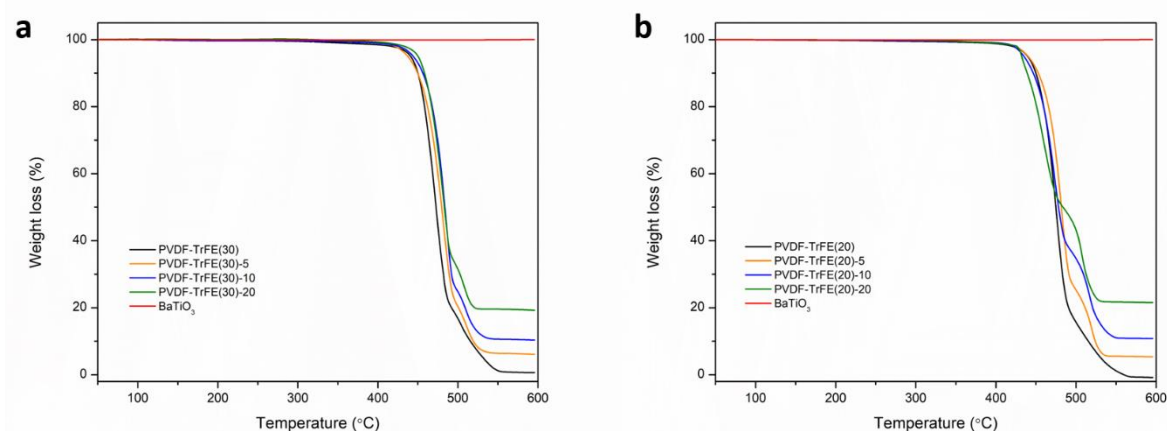


**Figure 5.** TGA curves of (a) PVDF-TrFE(30)-BaTiO<sub>3</sub> foams and (b) PVDF-TrFE(20)-BaTiO<sub>3</sub> foams.

**Table 4.** TGA data of PVDF-TrFE/BaTiO<sub>3</sub> composite foams

Sample code	T <sub>onset</sub> [°C]	W <sub>res</sub> <sup>a</sup> [%]
PVDF-TrFE(30)	452	0.6
PVDF-TrFE(30)-5	457	6.1
PVDF-TrFE(30)-10	464	10.3
PVDF-TrFE(30)-20	460	19.2
PVDF-TrFE(20)	455	0.2

PVDF-TrFE(20)-5	462	5.3
PVDF-TrFE(20)-10	451	10.8
PVDF-TrFE(20)-20	435	21.5

<sup>a</sup>At 600°C

DSC thermograms of the PVDF-TrFE/BaTiO<sub>3</sub> composite foams are shown in Figure 6 and all relevant calorimetric data are collected in Table 5. During the first heating scan (Figure 6a and 6c), three endothermic peaks are clearly observed for all the investigated samples. As reported in the literature, the first peak (positioned around 50 °C) could be ascribed to order/disorder processes associated with molecular conformations at the crystallite surface in PVDF copolymers containing up to 35 mol% TrFE units.<sup>39</sup> At this temperature, the molecular mobility on the crystallites' surface increases, leading to conformational reorganization in the crystalline and/or paracrystalline regions in PVDF-TrFE copolymers.<sup>39</sup> The second endothermic peak is attributed to ferroelectric (FE) to paraelectric (PE) transition occurring at Curie temperature ( $T_c$ ) around 90 °C and 120 °C in PVDF-TrFE(30) and PVDF-TrFE(20) composite foams, respectively. The Curie temperature varies based on the TrFE molar content in the corresponding copolymer. At higher molar contents, this temperature shifts to lower values.<sup>39,40</sup> The enthalpy of this second peak corresponds to the necessary energy for the FE → PE transition and is related to the energy difference between the crystalline structures involved in the process.<sup>41</sup> From the collected data in Table 5, it could also be noticed that higher enthalpies ( $\Delta H_c$ ) are identified in the PVDF-TrFE(20) samples when compared to those of PVDF-TrFE(30) composite foams. This can be related to the more ordered crystal phase in PVDF-TrFE(20) composites, as previously confirmed by the XRD analysis. Additionally, the Curie transition enthalpy in composite foams increased with the addition of ceramic filler, reaching its highest value in samples containing 20 wt% of BaTiO<sub>3</sub>. This effect was more pronounced in PVDF-TrFE(30) composite foams. The melting endotherms were observed around 140 °C in all composite foams, representing the melting of the paraelectric  $\alpha$  phase. The corresponding melting enthalpies in PVDF-TrFE(30) composite foams are slightly lower compared to the melting enthalpies of the PVDF-TrFE(20) composites. This finding also nicely corroborates the data obtained from the XRD analysis. In the second heating scans (Figure 6b and 6d), the peak at around 52 °C (previously detected in the first heating scans) is absent, while the Curie transition peaks and melting peaks in both

copolymers are shifted to higher temperatures (Table 5), diminishing the presence of the developed  $\beta$  phase during the crystallization process.<sup>42</sup>

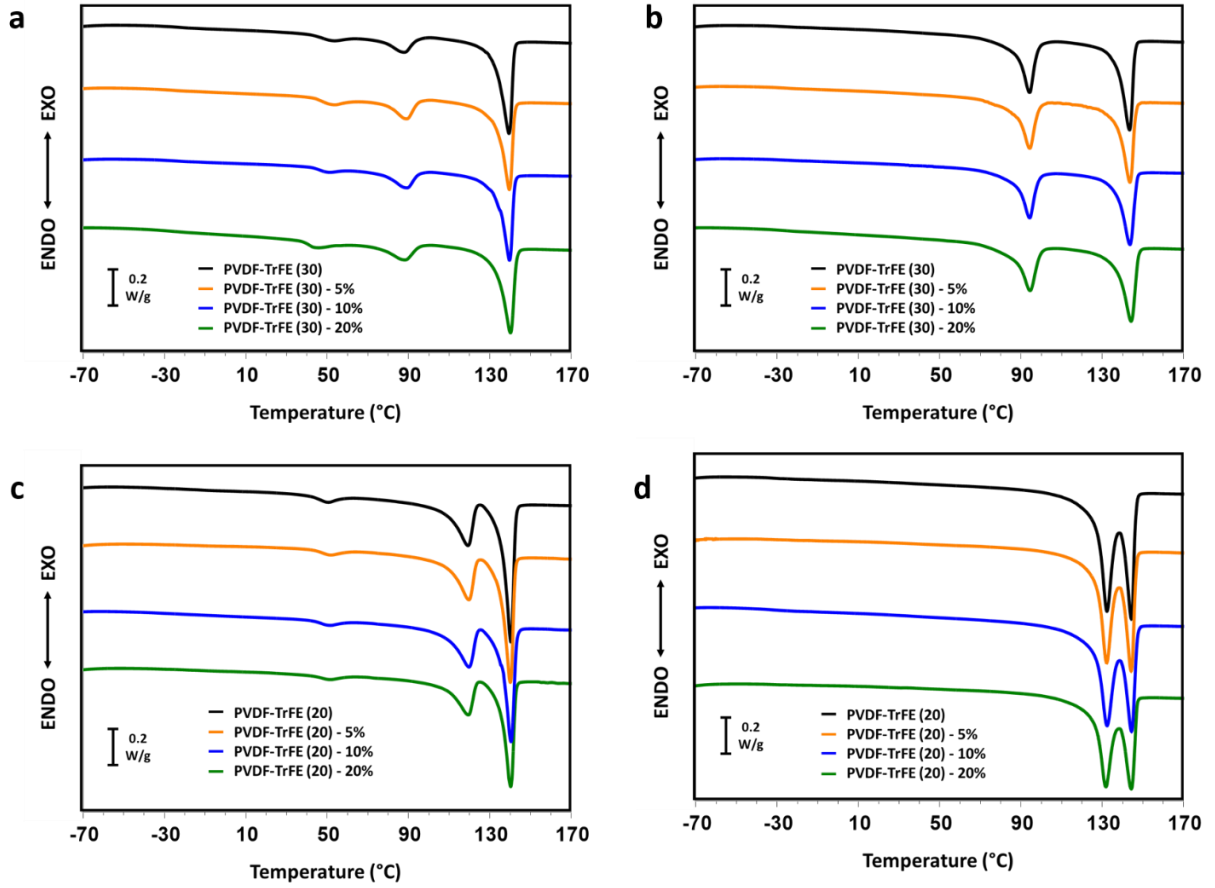


**Figure 6.** DSC first heating scans of PVDF-TrFE(30)/BaTiO<sub>3</sub> composite foams (a) and PVDF-TrFE(20)/BaTiO<sub>3</sub> composite foams (c). DSC second heating scans after controlled cooling of PVDF-TrFE(30)/BaTiO<sub>3</sub> composite foams (b) and PVDF-TrFE(20)/BaTiO<sub>3</sub> composite foams (d).

**Table 5.** Calorimetric data of PVDF-TrFE/BaTiO<sub>3</sub> composite foams.



Sample code	I heating scan					II heating scan			
	T <sub>1p</sub> [°C]	T <sub>c</sub> [°C]	ΔH <sub>c</sub> <sup>a</sup> [J g <sup>-1</sup> ]	T <sub>m</sub> [°C]	ΔH <sub>m</sub> <sup>b</sup> [J g <sup>-1</sup> ]	T <sub>c</sub> [°C]	ΔH <sub>c</sub> <sup>c</sup> [J g <sup>-1</sup> ]	T <sub>m</sub> [°C]	ΔH <sub>m</sub> <sup>b</sup> [J g <sup>-1</sup> ]
PVDF-TrFE(30)	53	88	8.2	139	25.0	94	21.0	143	26.1
PVDF-TrFE(30)-5	53	89	9.9	140	25.6	94	20.9	144	26.6
PVDF-TrFE(30)-10	51	89	10.3	140	25.9	94	21.4	144	26.4
PVDF-TrFE(30)-20	45	88	11.6	140	31.1	94	26.1	144	32.5
PVDF-TrFE(20)	50	119	21.4	140	28.0	132	44.2	144	22
PVDF-TrFE(20)-5	52	120	21.7	140	27.4	132	44.1	144	22.2
PVDF-TrFE(20)-10	52	120	21.7	141	27.4	132	45.7	144	21.8
PVDF-TrFE(20)-20	52	120	21.1	140	27.6	132	44.8	144	22.3

<sup>a</sup> Enthalpy per gram of polymer, referred to the second endotherm peak (FE-PE transition) in the first heating scan.

<sup>b</sup> Enthalpy per gram of polymer, referred to the last endotherm peak (melting of PE phase).

<sup>c</sup> Enthalpy per gram of polymer, referred to the first endotherm peak (FE-PE transition) of the second heating scan.

### 3.5 Piezoelectric properties

Despite the high content of  $\beta$  phase in PVDF-TrFE copolymers and the addition of BaTiO<sub>3</sub> particles in the composites, the alignment of the ferroelectric domains is crucial for a macroscale piezoelectric behavior of the foams.<sup>43</sup> For efficient polarization, the poling process is usually carried out at the Curie temperature (T<sub>c</sub>) of the piezoelectric material. BaTiO<sub>3</sub> has a Curie temperature of 120 °C,<sup>44</sup> very similar to that of PVDF-TrFE(20), while T<sub>c</sub> of PVDF-TrFE(30) is significantly lower (see Table 5). An important aspect to consider in the poling process of the investigated composite foams is the opposite polarity of PVDF-TrFE copolymers and BaTiO<sub>3</sub>. Since the piezoelectric coefficients have opposite signs, when poled under the same electric field it is expected that their piezoelectric activities partially cancel. Conversely, the use of two opposite-sign electric fields in the poling phase enables the synergic exploitation of both piezoelectric components (BaTiO<sub>3</sub> and PVDF-TrFE). By taking into account the Curie temperatures of the tested materials, the PVDF-TrFE(20)/BaTiO<sub>3</sub> foams were poled at 120°C under the same electric field, while the PVDF-TrFE(30)/BaTiO<sub>3</sub> were poled by a two-step process, since the T<sub>c</sub> of PVDF-TrFE(30) and BaTiO<sub>3</sub> are remarkably different. More precisely,

first, the BaTiO<sub>3</sub> was poled at 120 °C and, subsequently, the PVDF-TrFE(30) was poled at 100 °C, after changing the direction of the applied electric field.

The piezoelectric properties of the composite foams were investigated in terms of piezoelectric strain coefficient  $d_{33}$  and output current. For each specimen, the corresponding  $d_{33}$  values are reported in Table 6 and the correlation between the  $d_{33}$  coefficient and the weight percentage of BaTiO<sub>3</sub> is presented in Figure 7. The measurement of the piezoelectric strain coefficient were repeated three times for each specimen, with a maximum standard deviation value equal to 14.8 %. In the case of pure PVDF-TrFE foams, the two aforementioned polarization processes led to similar  $d_{33}$  values for PVDF-TrFE(30) (-18.7 pC N<sup>-1</sup>) and for PVDF-TrFE(20) (-19.2 pC N<sup>-1</sup>). On the other hand, by increasing the BaTiO<sub>3</sub> content, the two distinct effects of the different polarization methods were clearly observable. The  $d_{33}$  absolute value of the PVDF-TrFE(20) composite foams decreases with the addition of BaTiO<sub>3</sub> particles and presents its minimum value in the case of PVDF-TrFE(20)-20 composite foam (-10.1 pC N<sup>-1</sup>). This result is the consequence of the opposite polarity of BaTiO<sub>3</sub> and PVDF-TrFE, where the positive polarization electric field (+20 kV/mm) led to a distribution of the BaTiO<sub>3</sub> ferroelectric domains which contrasts the effects of the PVDF-TrFE(20) dipoles and negatively impacts on the macroscale piezoelectric strain coefficient of the specimen. Similar results implying this negative impact of ceramic filler were reported by several authors.<sup>45,46</sup>

The two-step polarization method adopted for the PVDF-TrFE(30) composite foams led to a different result. As observable in Figure 7, the higher the content of BaTiO<sub>3</sub> the higher the absolute value of the  $d_{33}$  of the PVDF-TrFE(30) composite foams (up to -28.3 pC N<sup>-1</sup> in the case of 20 wt.% of BaTiO<sub>3</sub>). This trend clearly demonstrates the effectiveness of such a poling technique, which allows to fully exploit the contribution of both the piezoelectric components (PVDF-TrFE(30) and the BaTiO<sub>3</sub>).

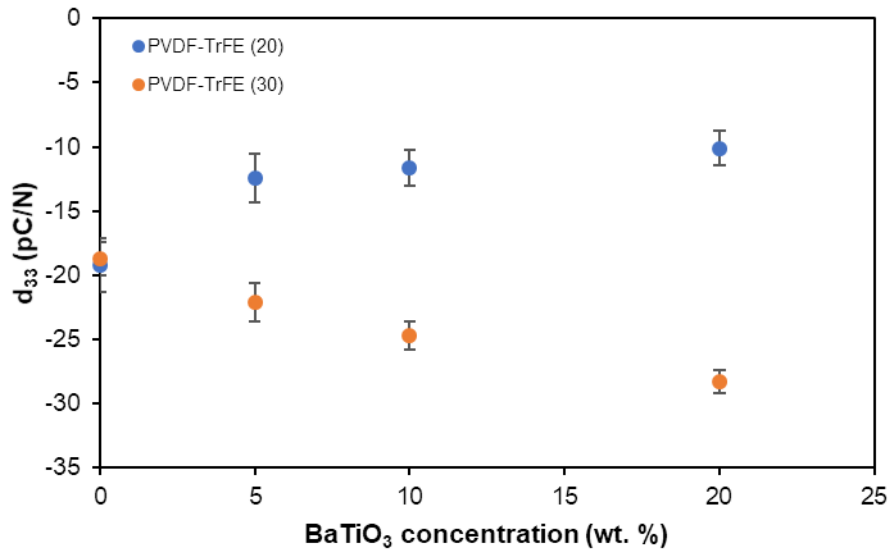


**Figure 7.** Piezoelectric strain coefficient ( $d_{33}$ ) of PVDF-TrFE -BaTiO<sub>3</sub> composite foams.

**Table 6.** Piezoelectric strain coefficient ( $d_{33}$ ) of PVDF-TrFE/BaTiO<sub>3</sub> composite foams.

Sample code	$d_{33}$ [pC N <sup>-1</sup> ]
PVDF-TrFE(30)	-18.7
PVDF-TrFE(30)-5	-22.1
PVDF-TrFE(30)-10	-24.7
PVDF-TrFE(30)-20	-28.3
PVDF-TrFE(20)	-19.2
PVDF-TrFE(20)-5	-12.4
PVDF-TrFE(20)-10	-11.6
PVDF-TrFE(20)-20	-10.1

Furthermore, the piezoelectric output current was measured for each polarized specimen according to the setup represented in Figure 1b. Their values are plotted for three different frequencies (2, 5 and 10 Hz) in the graphs of Figure 8a and Figure 8b for the PVDF-TrFE(30) and PVDF-TrFE(20) composite foams, respectively. Overall, the current amplitude presents an

increasing trend with the frequency of the compressive force, consistently with the definition of the output current of a piezoelectric material:

$$I_p = d_{33} \frac{dF}{dt} \quad (4)$$

The measured peak-to-peak values of the piezoelectric current reflect the trends observed for the  $d_{33}$  results. Indeed, the lowest current amplitude is measured for the PVDF-TrFE(20) composite foam with 20 wt.% of BaTiO<sub>3</sub>, which was poled with the single-step polarization method (current peak-to-peak value equal to 60.9 nA, at 10 Hz). On the other hand, the maximum value of the piezoelectric output current was measured for the PVDF-TrFE(30) composite foam with 20 wt.% of BaTiO<sub>3</sub> (130 nA, at 10 Hz), which is the one with the highest  $d_{33}$  value. These results represent a further demonstration of the possibility to achieve enhanced piezoelectric responses by adopting a polarization method able to synergically conjugate the effects of both the piezoelectric components, PVDF-TrFE and BaTiO<sub>3</sub>.

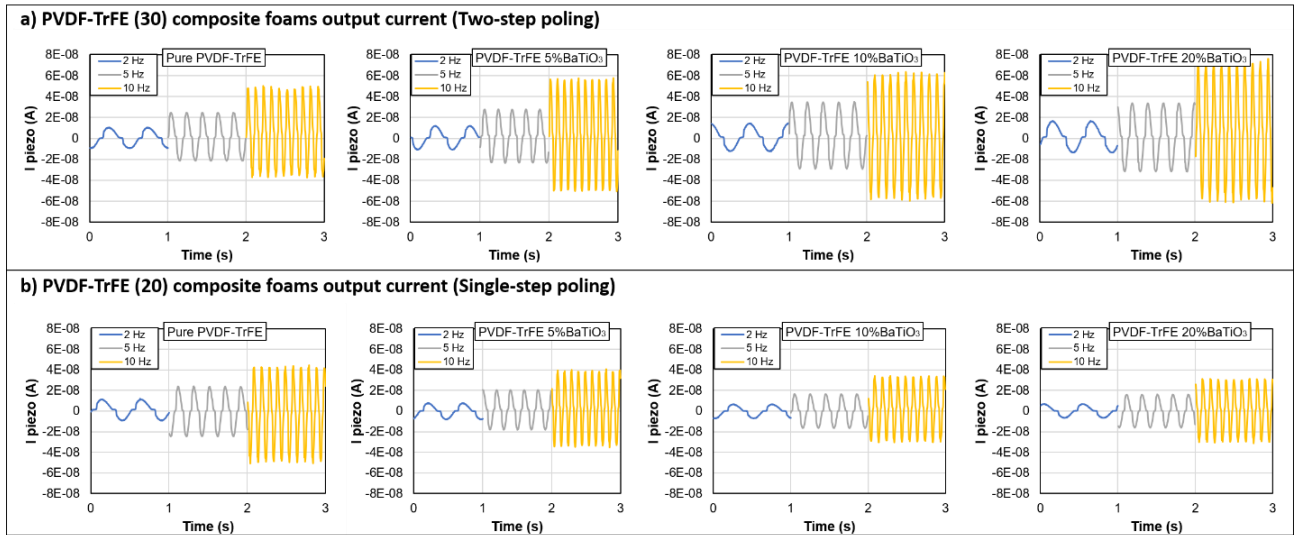


**Figure 8.** Current measurements of (a) PVDF-TrFE(30) -BaTiO<sub>3</sub> composite foams and (b) PVDF-TrFE(20) -BaTiO<sub>3</sub>.

With the aim to further investigate the behavior of the piezoelectric foams, an accelerated fatigue test was carried out on the PVDF-TrFE(30) foam with 20 wt.% of BaTiO<sub>3</sub>, polarized with the two-step poling method. This specific foam was selected as it presents the highest  $d_{33}$  value (i.e., -28.3 pC/N) and eventual variations on the current amplitude could be clearly visible. The

fatigue test was performed by applying a sinusoidal compressive force oscillating between 0 N and 80 N at 10 Hz frequency for 105 cycles.

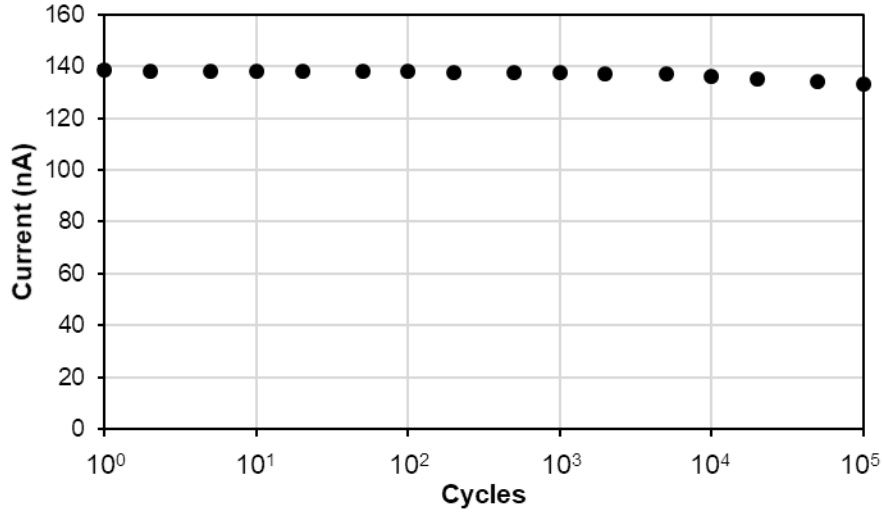


**Figure 9.** Fatigue test of the PVDF-TrFE(30) foam with 20 wt.% of BaTiO<sub>3</sub>, polarized with the two-step poling method. The test was carried out at 10 Hz by applying a sinusoidal load oscillating between 0 N and 80 N.

The output current was measured for each cycle according to the setup described in Section 2.5. As observable from the graph of Figure 9, the peak-to-peak piezoelectric current shows a slight decreasing trend, and after 105 cycles the current amplitude is equal to 133.2 nA, which corresponds to a reduction of 4% of the initial one.

#### 4 CONCLUSIONS

PVDF-TrFE/BaTiO<sub>3</sub> composite foams with enhanced piezoelectric response were successfully prepared using TIPS method. Two different poling procedures have been applied due to the different molar content of the used copolymers. All foams consisted of open-cell pores in micron size, have low density, and high porosity (up to 94.6%). The structural analysis showed that the prepared foams crystallized mainly in  $\beta$  crystal phase, while the addition of the ceramic particles

resulted in higher crystallinity (up to 74.5%) and improved thermal stability. The piezoelectric strain coefficient ( $d_{33}$ ) and output current reached the highest value of  $-28.3 \text{ pC N}^{-1}$  and 130 nA for the PVDF-TrFE(30)-20 composite. The improved piezoelectric response confirmed the success of the two-step poling method, in which both components are polarized in the same direction, thus contributing to the higher piezoelectric response compared to the pure copolymer. These results provide a simple and cost-effective technique to fabricate lightweight and flexible piezoelectric composites with improved piezoelectric response, suitable for energy harvesting and sensing applications.

## ACKNOWLEDGMENT

This work was financially supported by NATO grant -Project number NATO SPS G5772.

## CONFLICT OF INTEREST

The authors declare no conflict of interest.

## REFERENCES

- [1] S. Das Mahapatra, P.C. Mohapatra, A.I. Aria, G.Christie, Y.K.Mishra, S.Hofmann, V.K. Thakur, *Adv. Sci.* **2021**, 8, 2100864.
- [2] S. Mishra, L. Unnikrishnan, S. K. Nayak, S. Mohanty, *Macromol. Mater. Eng.* **2019**, 304, 1800463.
- [3] S.Labihi, N.Chakhchaoui, A. Eddiai, M. El Achaby, M. Meddad, O.Cherkaoui, M. Mazroui, *Polym. Compos.* **2023**, 44, 2296.
- [4] S. S. Phadkule, S.Sarma, *Polym. Compos.* **2023**, 44, 1381.
- [5] M. C. Bertolini, S. Dul, E. C. L.Pereira, B. G. Soares, G. M. O. Barra, A.Pegoretti, *Polym.Compos.* **2021** 42, 6621.
- [6] Y. Hou, Y. Deng, Y. Wang, H. L. Gao, *RSC Adv.* **2015**, 5, 72090.
- [7] M. S. Sebastian, A. Larrea, R. Goncalves, T. Alejo, J.L. Vilas, V. Sebastian, P. Martins, S. Lanceros-Mendez, *RSC Adv.* **2016**, 6, 113007.
- [8] Z. Y. Wang, H. Q. Fan, K. H. Su, X. Wang, Z. Y. Wen, *Polymer (Guildf).* **2007**, 48, 3226.
- [9] X. Chen, J. Shao, X. Li, H. Tian, *IEEE Trans. Nanotechnol.* **2016**, 15, 295.

- [10] F. Oliveira, Y. Leterrier, O. Sereda, A. Neels, A. Dommann, D. Damjanovic, *J. Polym. Sci. Part B Polym. Phys.* **2014**, *52*, 496.
- [11] D. Guo, I. Stolichnov, N. Setter, *J. Phys. Chem. B* **2011**, *115*, 13455.
- [12] W. Zhang, B. Zaarour, L. Zhu, C. Huang, B. Xu, X.A. Jin, *J. Eng. Fiber. Fabr.* **2020**, *15*, 1.
- [13] J. Yan, M. Lui, Y.G. Jeong, W. Kang, L. Li, Y. Zhao, N. Deng, B. Cheng, G. Yang, *NanoEnergy* **2019**, *56*, 662.
- [14] C. K. Jeong, C. Baek, A. I. Kingon, K. Il Park, S. H. Kim, *Small* **2018**, *14*, 1.
- [15] Z. Zhou, Z. Zhang, Q. Zhang, H. Yang, Y. Zhu, Y. Wang, L. Chen, *ACS Appl. Mater. Interfaces* **2020**, *12*, 1567.
- [16] Y. Tong, L. Li, J. Liu, Y. Li, *Polym. Compos.* **2019**, *40*, 4742.
- [17] Z. Hua, X. Shi, Y. Chen, *Polym. Compos.* **2017**, *40*, E177.
- [18] X. Chen, X. Li, J. Shao, N. An, H. Tian, C. Wang, T. Han, L. Wang, B. Lu, *Small* **2017**, *13*, 1.
- [19] X. Hu, X. Yan, L. Gong, F. Wang, Y. Xu, L. Feng, D. Zhang, Y. Jiang, *ACS Appl. Mater. Interfaces* **2019**, *11*, 7379.
- [20] D. Chen, T. Sharma, J. X. J. Zhang, *Sensors Actuators, A Phys.* **2014**, *216*, 196.
- [21] D. Chen, K. Chen, K. Brown, A. Hang, J. X. J. Zhang, *Appl. Phys. Lett.* **2017**, *110*, 153902.
- [22] A. M. Mohamed, K. Yao, Y. M. Yousry, J. Wang, S. Ramakrishna, *J. Appl. Phys.* **2020**, *127*, 214102.
- [23] Y. Cui, Y. Liu, Y. Cui, X. Jing, P. Zhang, X. Chen, *Acta Biomater.* **2009**, *5*, 2680.
- [24] A. Bužarovska, *J. Mater. Sci.* **2017**, *52*, 12067.
- [25] A. Bužarovska, C. Gualandi, A. Parrilli, M. Scandola, *Composites Part B*, **2015**, *81*, 189.
- [26] A. Arrigoni, L. Brambilla, C. Bertarelli, G. Serra, M. Tommasini, C. Castiglioni, *RSC Adv.* **2020**, *10*, 37779.
- [27] G. Cortili, G. Zerbi, *Spectrochim. Acta Part A Mol. Spectrosc.* **1967**, *23*, 285.
- [28] R. Gregorio, *J. Appl. Polym. Sci.* **2006**, *100*, 3272.
- [29] A. C. Lopes, C. M. Costa, C. J. Tavares, I. C. Neves, S. Lanceros-Mendez, *J. Phys. Chem. C* **2011**, *115*, 18076.
- [30] C. Wan, C. R. Bowen, *J. Mater. Chem. A* **2017**, *5*, 3091.
- [31] R. Gregorio, M. Cestari, *J. Polym. Sci. Part B Polym. Phys.* **1994**, *32*, 859.
- [32] J. Kim, J. H. Lee, H. Ryu, J. H. Lee, U. Khan, H. Kim, S. S. Kwak, S. W. Kim, *Adv. Funct. Mater.* **2017**, *27*, 1.

- [33] A. J. Lovinger, T. Furukawa, G. T. Davis, M. G. Broadhurst, *Polymer (Guildf)*. **1983**, 24, 1733.
- [34] P. Taylor, K. Tashiro, M. Kobayashi, *Phase Transitions*, **1989**, 18, 213.
- [35] J. Q. Qi, T. Peng, Y. M. Hu, L. Sun, Y. Wang, W. P. Chen, L. T. Li, C. W. Nan, H. L. W. Chan, *Nanoscale Res. Lett.* **2011**, 6, 1.
- [36] R. I. Haque, R. Vie, M. Germainy, L. Valbin, P. Benabeh, X. Boddaert, *Flex. Print. Electron.* **2016**, 1, 015001.
- [37] N. Ogata, *J. Macromol.Sci., Part C: Polym.Rev.* **2007**, 42, 399.
- [38] S. F. Mendes, C. M. Costa, C. Caparros, V. Sencadas, S. Lanceros-Méndez, *J. Mater. Sci.* **2012**, 47, 1378.
- [39] G. Teyssèdre, C. Lacabanne, *Ferroelectrics* **1995**, 171, 125.
- [40] C. Leonard, J. L. Halary, L. Monnerie, F. Micheron, *Polym. Bull.* **1984**, 11, 195.
- [41] R. Gregorio, M. M. Botta, *J. Polym. Sci. Part B Polym. Phys.* **1998**, 36, 403.
- [42] C. J. L. Constantino, A.E. Job, R.D. Simoes, J. A. Giacometti, V. Zucolotto, O.N. Oliveira, G. Gozzi, D. L. Chinaglia, *Appl. Spectrosc.* **2005**, 59, 275.
- [43] G. Selleri, M. E. Gino, L. Gasperini, M. Zanoni, C. Gualandi, M. L. Focarete, D. Fabiani, *Annu. Rep. - Conf. Electr. Insul. Dielectr. Phenomena, CEIDP* **2021**, 2021-December, 61.
- [44] K. Sakayori, Y. Matsu, H. Abe, E. Nakamura, M. Kenmoku, T. Hara, D. Ishikawa, A. Kokubu, K. Hirota, T. Ikeda, *Jpn. J. Appl. Phys.* **1995**, 34, 5443.
- [45] P. Taylor, H. L. W. Chan, M. C. Cheung, C. L. Choy, *Ferroelectrics* **1999**, 224, 113.
- [46] K. L. Ng, *IEEE Trans. Ultrason. Ferroelectr. Freq. Control* **2000**, 47, 1308.